Targeting TGFβ signaling pathway in fibrosis and cancer

Karkampouna, S.

Appendix I

Role of type III receptor, CRIPTO, in injury-induced liver regeneration and hepatocellular carcinoma

Sofia Karkampouna[1*], Danny van der Helm[2*], Peter ten Dijke[1], Hein Verspaget[2], Minneke Coenraad[2], Marianna Kruithof-de Julio[1,3,#]

[1]Department of Molecular and Cell Biology, Leiden University Medical Center, Leiden, the Netherlands,
[2]Department of Gastroenterology and Hepatology, Leiden University Medical Center, Leiden, the Netherlands,
[3]Department of Urology, Leiden University Medical Center, Leiden, the Netherlands
[*] Equally contributed, [#] Corresponding author

Manuscript in preparation

Abstract

Hepatocellular carcinoma (HCC) is the third cause of cancer- related death with a growing incidence worldwide. A comprehensive view of the mechanism initiating the switch from liver regeneration to liver failure and tumor formation is needed. Here we report on studies regarding the potential role of a Transforming growth factor β (TGFβ) family member, the type III receptor for NODAL ligand, CRIPTO, in adult liver disease progression. We investigated the expression status of CRIPTO and its interaction partners *in vivo* in an acute liver injury mouse model and examined the *in vivo* effects on liver regeneration of adenoviral-mediated CRIPTO overexpression. Liver tissue specimens from HCC patients were evaluated for CRIPTO protein expression. Induction of Cripto was observed after experimental liver injury in mice and induction of Cripto overexpression caused bile duct reaction and hepatic progenitor cell activation. Both transient and stable CRIPTO overexpression in human hepatoma HepG2 cells led to upregulation of liver progenitor cell activity, epithelial-to-mesenchymal transition (EMT), increased expression of EMT and cancer stem cell markers along with enhancement of cell proliferation and migration. The majority of human HCC tumor samples exhibit high levels of CRIPTO as compared to the non-tumorous counterpart tissue from the same patients. Overall, our preliminary data suggest CRIPTO as potential driver of liver progenitor activation during liver injury and possibly of human HCC progression.

Introduction

Hepatocellular carcinoma (HCC) accounts for the majority of primary liver cancer cases and is the sixth common type of cancer[1]. HCC arises in the majority of cases on a background of cirrhosis, which may be caused by chronic exposure to damaging factors, such as alcohol, or viral hepatitis (HBV, HCV)[2]. Systemic treatment available is the tyrosine kinase RAF inhibitor, sorafenib, which delays HCC progression and metastasis and is indicated for advanced tumors or tumors progressing upon loco-regional therapies[3,4]. There are no clinical or biochemical biomarkers available to identify responders to sorafenib[4]. Many other compounds have been tested in recent years, but none of them has proven to be superior to sorafenib yet[5]. Circulating TGFβ and α-fetoprotein (AFP) levels have been explored as biomarkers in HCC[6]. AFP is reactivated in pathological conditions and is considered a marker of liver progenitor cells (oval cells)[7]. However, detection of high levels of AFP cannot be used for diagnosis or prognosis as it does not predict tumor size, stage and HCC progression and is absent in 30% of HCC cases[6]. Signaling from Transforming growth factor β (TGFβ) pathway is an established regulator of liver homeostasis with tumor suppressor role during early tumor development[8]. As with other types of cancer, TGFβ exerts tumor promoter effects on established primary tumors and enhances epithelial-to-mesenchymal transition (EMT), cell motility and invasion contributing to metastases formation[9].

High levels of circulating TGFβ have been detected in HCC patients with a small HCC[10] although mutations in TGFβ pathway members have low prevalence in HCC. High levels of SMAD7[11], downregulation of TGFβ receptor type I and II expression[12,13] and high levels of SMAD4 have been associated with poor prognosis in HCC patients[14]. SMAD3-mediated NODAL signaling has been linked to increased EMT and HCC cell invasion via a mechanism involving pluripotency transcription factor NANOG[15]. NANOG induces NODAL/CRIPTO expression and correlates with HCC metastasis and poor survival. NODAL and CRIPTO are involved in plasticity of tumor cells, cancer-stem cell maintenance and metastasis[16,17]. CRIPTO is an oncofetal protein suggested to partially promote tumorigenesis by inhibiting TGFβ signaling[18-20] and is involved in the crosstalk of TGFβ/ NODAL pathways with p38/ c-Jun N-terminal kinase (JNK), sarcoma viral oncogene (c-SRC)/ Mitogen-activated protein kinase (MAPK)/ protein kinase B thymoma oncogene (AKT) and Wingless type (WNT) signaling pathways[21-23]. CRIPTO is silenced postnatally and re-expression is often associated with pathological conditions such as neoplasias of breast, lung, prostate, ovarian, bladder, colon, skin, lung and brain[15,24-32]. NODAL-independent CRIPTO signaling is mediated through the heat shock glucose-regulated protein (GRP78), which promotes c-SRC/MAPK/AKT activation. This pathway is oncogenically mutated in liver cancer[33]. Moreover, liver-specific deletion of GRP78 indicated a homeostatic and protective role during endoplasmic reticulum-stress response while elevated GRP78 levels are associated with HCC progression[34-36]. In the present study we investigated the role of CRIPTO-associated pathways NODAL and GRP78 aiming to identify novel TGFβ-related regulators of liver regeneration and HCC progression.

Materials and Methods

Human specimens

Liver tissue was obtained from resected livers during orthotopic liver transplantation. Paraffin embedded HCC and non-tumor tissue of anonymous patients transplanted for HCC in the setting of alcoholic liver disease (ALD) or viral hepatitis C (HCV) etiology were randomly selected. Selection of tissues was performed in agreement with the "code of good practice".

Acute liver damage model and administration of adenovirus

Animal protocols were in full compliance with the guidelines for animal care and were approved by the Leiden University Medical Center Animal Care Committee. Acute liver injury was induced in 5-6 weeks old male C57Bl6 mice weighing 20- 25 g by intraperitoneal injection of a single dose of 1 ml/kg body weight carbon tetrachloride (CCl_4) (Sigma, from a 50% solution mixed in mineral oil) or mineral oil (control). Mice were sacrificed at 3, 6, 24, 48, 72 hours and day 6 (n=2- 3 per time point).
Adenoviral constructs expressing β-galactosidase (lacZ) or Cripto were prepared using the Gateway adenoviral expression vectors pAd/CMV/V5-lacZ or pAd/CMV/V5-DEST, mouse Cripto expression plasmid was a gift from from Dr. Peter Gray [18]. AdlacZ (AdCon) or AdCripto (1x10E+9 viral particles/ mouse) was injected intravenously via the tail vein to enhance delivery to the liver[37]. After 24 hours, CCl_4 was intraperitoneally injected (day 0). Treatment groups were as follows: AdlacZ, CCl_4+AdlacZ, AdCripto, CCl_4+AdCripto. At day 1, day 2 and day 3 after CCl_4 administration mice were sacrificed and liver tissues were collected for histology preparation, RNA/ protein isolation and analysis.

Immunofluorescence

Liver tissues were fixed in 4% paraformaldehyde solution overnight, washed in phosphate buffer saline (PBS) and processed for paraffin embedding. For every mouse, one of the liver lobules was embedded in a paraffin block and multiple serial sections (6 μm) were prepared. From the human tissue, serial sections of 4 μm were prepared. For antigen retrieval, sections were boiled 10-30 min in antigen unmasking solution (Vector Labs) and were incubated in 3% H_2O_2 for endogenous peroxidases sequestering. Sections were blocked with 1% bovine serum albumin in PBS-0.1% v/v Tween 20 and subsequently incubated with primary antibodies diluted in the blocking solution, overnight at 4°C or room temperature. Primary antibodies and dilutions used are as follows: anti-CRIPTO 1:2000 and anti-GRP78 1:1000 (kindly provided by Dr. Peter Gray), anti-αSMA 1:500 (Sigma). Next day, sections were incubated with secondary antibodies labeled with Alexa Fluor 488, 555, or 647 (Invitrogen/Molecular Probes, 1:250 in PBS-0.1% Tween-20). Detection of CRIPTO and GRP78 was enhanced using tyramide amplification (Invitrogen/ Molecular Probes) as described previously[38]. All sections were counterstained with TO-PRO-3 (Invitrogen/Molecular Probes) at 1:1000 dilution in PBS-0.1% Tween-20 for nuclei visualization, and mounted with Prolong G mounting medium (Invitrogen/ Molecular Probes). All immunofluorescence experiments were repeated multiple times using different sections from the same lobule of every mouse.

RNA isolation, RT-PCR and Quantitative PCR

During liver tissue collection, one of the liver lobules of each individual mouse was snapfrozen in liquid nitrogen and stored at -80°C for RNA analyses. Tissue (100 mg) was homogenized using an UltraTurrax homogenizer (T25 basic, IKA) in TRIpure reagent (Roche) and directly processed for total RNA isolation according to the TRIpure RNA extraction protocol. Total RNA (0.5 µg) was used for first strand cDNA synthesis using RevertAid H Minus first strand cDNA synthesis kit (Fermentas). For quantitative PCR (Q-PCR) ten-fold diluted cDNA was amplified in a CFX Real Time Detection system (Bio-rad) using SYBR Green Supermix reagent (Bio-rad). Expression levels were normalized to housekeeping gene β-actin.
Primer sequences:

β-actin (human): for-, AATGTCGCGGAGGACTTTGATTGC,
rev- GGATGGCAAGGGACTTCCTGTAAA
β-actin (mouse): for- GGGGTGTTGAAGGTCTCAAA, rev- AGAAAATCTGGCACCCC
Ck19 (mouse): for- CCGGACCCTCCCGAGATTA, rev- CTCCACGCTCAGACGCAAG
Afp (mouse): for- CGATGTGTTGGCTGCAATGA, rev- GTGCCAGCAGACACTGATG
Cripto (mouse): for- CGCCAGCTAGCATAAAAGTG, rev- CCCAAGAAGTGTTCCCTGTG
GRP78 (human): for- GAACGTCTGATTGGCGATGC, rev- TCAACCACCTTGAACGGCAA
NODAL (human): for-CTTCTCCTTCCTGAGCCAACAAGAGG,
rev-GGTGACCTGGGACAAAGTGACAGTG
N-CADHERIN (human): for- CAGACCGACCCAAACAGCAAC,
rev- GCAGCAACAGTAAGGACAAACATC
E-CADHERIN (human): for- TTGACGCCGAGAGCTACAC, rev- GACCGGTGCAATCTTCAAA
VIMENTIN (human): for- CCAAACTTTTCCTCCCTGAACC, rev- CGTGATGCTGAGAAGTTTCGTTGA
OCT4 (human): for- GAGAACCGAGTGAGAGGCAACC, rev- CATAGTCGCTGCTTGATCGCTTG
NANOG (human): for- AATACCTCAGCCTCCAGCAGATG, rev- TGCGTCACACCATTGCTATTCTTC
BMI-1 (human): for- TCATCCTTCTGCTGATGCTG, rev- CCGATCCAATCTGTTCTGGT
CD44 (human): for- TGGCACCCGCTATGTCCAG, rev- GTAGCAGGGATTCTGTCTG
ALK4 (human): for- GCTCGAAGATGCAATTCTGG, rev- TTGGCATACCAACACTCTCG
LEFTY (human): for-CGAGTGGCTGCGCGTCCGCGA, rev- CGAGGCACAGCTGCACTTCTGCACC
ZEB-1(human): for- CCATATTGAGCTGTTGCCGC, rev- GCCCTTCCTTTCCTGTGTCA
ZEB-2 (human): for- GACCTGGCAGTGAAGGAAAA, rev- GGCACTTGCAGAAACACAGA
TWIST (human): for- GCCGGAGACCTAGATGTCATT, rev- TTTTAAAAGTGCGCCCCACG
SNAIL-2 (human): for- TGTGTGGACTACCGCTGC, rev- TCCGGAAAGAGGAGAGAGG
EPCAM (mouse): for- AGGGGCGATCCAGAACAACG, rev- ATGGTCGTAGGGGCTTTCTC

Cell lines

The HCC cell line, HepG2, were maintained in Dulbecco's Modified Eagle Media (DMEM) supplemented with 10% fetal calf serum and 1% penicillin/streptomycin. For adenovirus transduction, 200 multiplicity of infection (MOI) of high titer virus was incubated with the media for 24 hours. Migration, proliferation assays and mRNA analysis were performed at 48 hours after transduction.

Migration, measurement of metabolic rate MTS assay and wound healing assay

Transwell cell migration and aqueous soluble tetrazolium/ formazan (MTS) metabolic activity/ proliferation assay were performed as described in previous studies[39].
For the wound-healing assay 500.000 cells/ well of a 24- well plate were seeded. After 24 hours, the wound was made and culture medium was refreshed. Subsequently pictures were taken (4x magnification) at at 0, 24, 48 and 76- hour time points. Size of wound was measured with ImageJ software.

Microscopy and Image analysis

Confocal microscopy of labeled specimens was performed on a Leica TC-SP5 microscope with a 40X 1.4 NA oil-immersion objective. Series of Z stacks were collected and reassembled in Image J software (rsbweb.nih.gov/ij). Mean area fraction fluorescence was calculated in Image J software using threshold to select the root boundary and measuring the percentage of positive surface inside the intensity defined by the threshold. For quantifications of immunofluorescence signal, staining experiments were performed on all the samples simultaneously to reduce technical variation and imaged using identical exposure and recording settings.

Statistical analysis

Statistical analysis was performed using GraphPad Prism 5.0 sofware (San Diego, CA) and two-way ANOVA tests. Data are presented as mean±SEM. Statistically significant differences are indicated with asterisks (* $P< 0.05$, ** $P<0.01$, *** $P<0.001$, ***$P<0.0001$). For quantitative PCR analysis experiments were repeated at least three times as technical replicates for every sample (different cDNA preparations using the RNA of one liver lobule per mouse or HepG2) and the average value was calculated. The mean values obtained from individual animals for every group (n=2-3) were used for ANOVA statistical analysis. For quantifications of immunofluorescence signal every stained section (representing one mouse liver sample) multiple fields of view were imaged and quantified (see section Microscopy and Image analysis). The average of these values was calculated for every mouse sample. Statistical analyses were performed on the values of all the mouse samples per treatment group (n=2-3 in total).

Results

Short term re-expression of Cripto after CCl_4-induced liver damage

To assess whether Cripto is involved in liver homeostasis we analysed its expression in normal and injury-induced regenerating liver tissues from wild type C57Bl6 male mice. As previously reported for other tissues[40], Cripto is not expressed postnatally in the liver under physiological conditions (**Fig.1A**). Cripto expression is induced during acute liver damage. A single CCl_4 injection leads to acute liver damage and fibrogenesis within the first 72 hours but is completely reversible within 6-7 days. In this model, a series of time points was analysed and Cripto protein expression was observed at 24 hours (**Fig.1A**). mRNA expression was induced within the first 3 hours after CCl_4 administration, with a peak of expression at 24

hours and a gradual downregulation from 48 hours onwards (**Fig.1B**).

***In vivo* overexpression of Cripto indicates progenitor cell activation**

Early induction of Cripto in response to tissue damage and localised expression around the damaged central vein area (**Fig.1A**) suggests a functional requirement. To further assess the function of Cripto we utilised the CCl_4-induced acute liver injury model in combination with adenoviral-mediated overexpression of mouse Cripto. At 24 hours prior to CCl_4 injection, the control adenovirus-lacZ (AdlacZ) or Cripto-adenovirus (Ad-Cripto) was administered to the 4 treatment groups AdlacZ, CCl_4+AdlacZ, AdCripto, CCl_4+AdCripto. Liver tissues were analysed at 24, 48 and 72 hours after CCl_4 administration. Histological analysis after Cripto overexpression indicated an aberrant number of bile ducts in the portal triad area (**Fig.1C)**. This area is not directly affected by CCl_4 (due to lack of metabolising enzymes) and is the site of residence of hepatic stem/progenitor, also termed as oval cells[41]. Each portal triad normally consists of the portal vein, the hepatic artery and one bile duct. The newly formed bile ducts indicate bile duct proliferation, and a process termed bile duct reaction due to liver progenitor (oval cell) activation[42]. In particular, the additional bile ducts (basal number is one bile duct; only the additional ducts are indicated) are positive for α-smooth muscle actin (αSMA) and were exclusively observed in liver tissues of the AdCripto and CCl_4+AdCripto groups (**Fig.1D**).

Cripto upregulation was detected at 24 hours in AdCripto or CCl_4+AdCripto mice (**Fig.1E**), exponentially upregulated at 48 hours (**Fig.1F**) and normalised back to the basal levels in all treatment groups (**Fig.1G)**. Next, we evaluated the expression of oval cell markers (AFP, cytokeratin 19 (CK19)) to test whether bile duct proliferation may be attributed to presence of oval cells. AFP expression (**Fig.1H-J**), measured in whole liver mRNA extracts, showed a pattern of transient upregulation similar to Cripto expression (**Fig.1E-G**), i.e., upregulated at 24 hours following AdCripto administration (**Fig.1H**), overall induced at 48 hours in all the treatment groups (**Fig.1I**) and reduced again after 72 hours. At this time point (72 hours), AFP levels remain elevated only in the CCl_4+AdCripto group (**Fig.1J**). CK19 expression was induced transiently early after CCl_4 administration at 24 hours (**Fig.1K-M**), preceding, but not after, the Cripto expression.

Further, transient overexpression by AdCripto was also validated *in vitro* in the HCC cell line HepG2. Upregulation of Cripto (**Fig.2A**) in the HepG2 led to induction of both interaction partners NODAL (**Fig.2B**) and GRP78 (**Fig.2C)**, mesenchymal markers N-CADHERIN and VIMENTIN (**Fig.2D-E**) as well as pluripotency/cancer stem cell (CSC) markers, Octamer binding transcription factor 4 (OCT4), homeobox transcription factor (NANOG), polycomb ring finger protein (BMI-1) and cell surface glucoprotein (CD44) (**Fig.2F-I**), were increased upon transient Cripto overexpression.

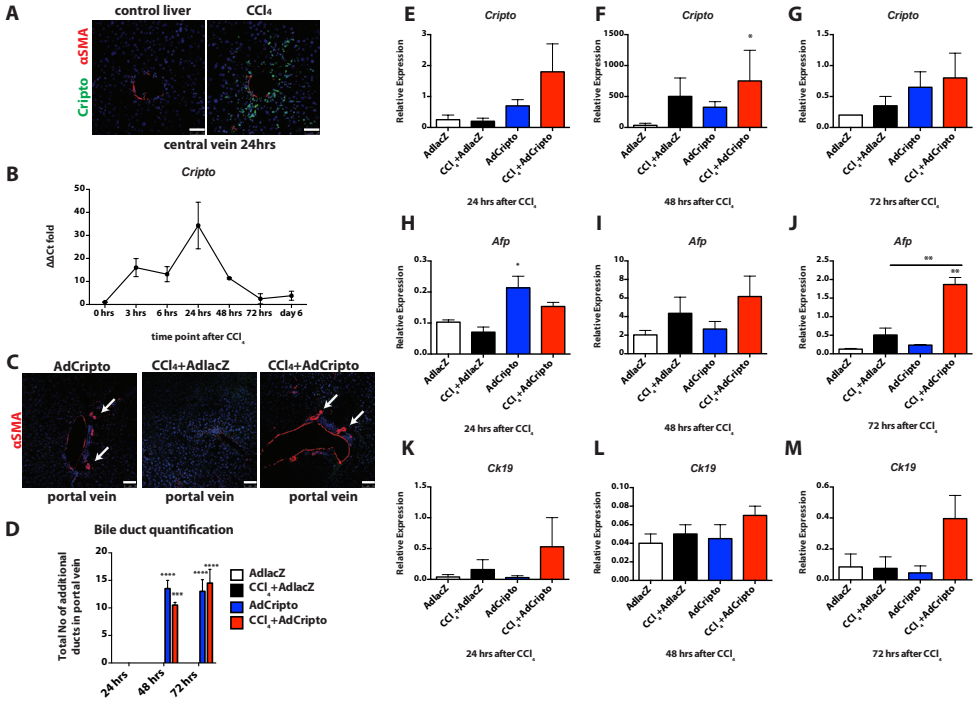

Fig.1. Cripto is re-expressed during early response of CCl_4-induced regeneration in mouse liver and may stimulate oval cell (progenitor) activation

(A). Immunofluorescence staining for Cripto (green) and αSMA (red) in liver tissue at 24 hours after vehicle or CCl_4 injection. Central vein area of the liver is depicted. Nuclei are stained with TO-PRO-3 (blue). Scale bars 50 μm. (B). *Cripto* mRNA expression in liver homogenates at different time points after CCl_4 treatment; 3 hours, 6 hours, 24 hours, 48 hours, 72 hours, 6 days. Values are normalized to *β-actin* and time point 0 hours (ΔΔCt fold). Error bars indicate SEM (n=3). (C). *In vivo* overexpression of Cripto was induced by adenovirus transduction in the acute CCl_4 liver injury model. Bile duct (oval progenitor cell-driven) reaction in the periportal area after overexpression of Cripto in the liver is depicted using immunofluorescence for αSMA (red) in livers administered with CCl_4+AdlacZ, CCl_4+AdCripto or AdCripto. Nuclei are stained with TO-PRO-3 (blue). Scale bars 75 μm. (D). Quantification of the additional bile ducts observed in the periportal vein area. Total number of additional bile ducts in 5 areas per section was averaged. Error bars indicate ±SEM (n=2). (E). *Cripto* mRNA expression in liver homogenates at 24 hours, 48 hours (F), 72 hours (G) after CCl_4 injection. Treatment groups: AdlacZ, CCl_4+AdlacZ, AdCripto, CCl_4+AdCripto. Values are normalized to *β-actin*. Error bars indicate SEM (n=3). (H). *A-fetoprotein* (*Afp*) (oval cell marker) mRNA expression in liver homogenates at 24 hours, (I). 48 hours and (J). 72 hours after CCl_4. (K). *Cytokeratin-19* (*Ck-19*) (oval cell marker) mRNA expression in liver homogenates at 24 hours, (L). 48 hours and (M). 72 hours after CCl_4. Treatment groups: AdlacZ, CCl_4+AdlacZ, AdCripto, CCl_4+AdCripto. Values are normalized to *β-actin*. Error bars indicate ±SEM (n=3).

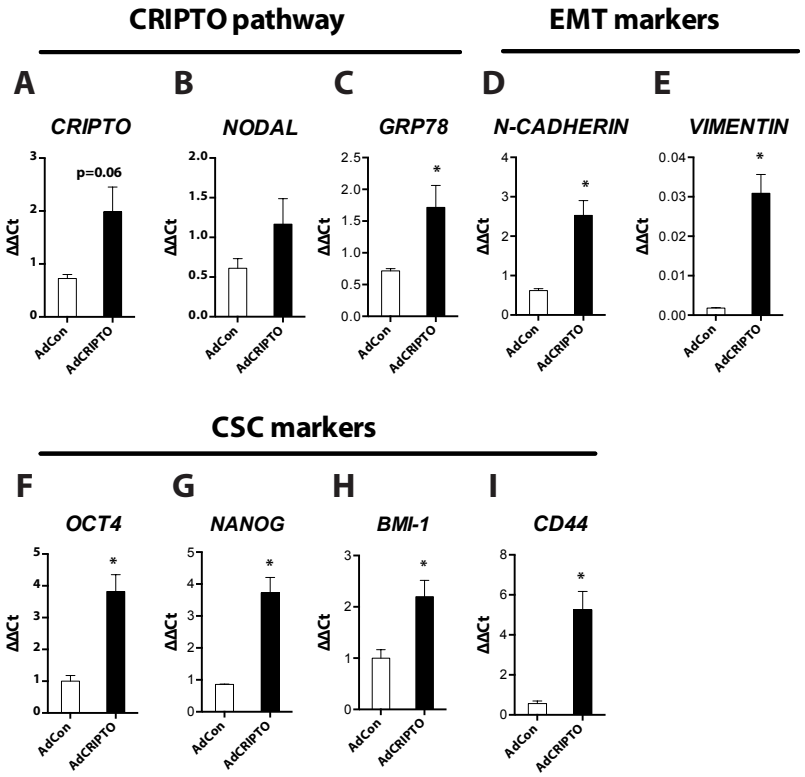

Fig.2. Effects of transient CRIPTO overexpression in EMT and stem cell marker induction
(A). Confirmation of expression of the CRIPTO adenoviral construct used previously *in vivo* and transient overexpression of CRIPTO in HepG2 cells; quantitative mRNA expression of *CRIPTO* and its interaction partners *NODAL* (B) and *GRP78* (C) in HepG2 cells 48 hours (hours) after transduction with control Adenovirus (AdCon) or CRIPTO expressing Adenovirus (AdCRIPTO). Error bars indicate ±SD (n=3). (D-E). mRNA expression levels of mesenchymal markers *NCADHERIN* and *VIMENTIN*. (F-I). mRNA expression levels of cancer stem cell (CSC) markers *OCT4* (F), *NANOG* (G), *BMI-1* (H), *CD44* (I) and in HepG2 cells 48 hours after transduction with control Adenovirus (AdCon) or CRIPTO expressing Adenovirus (AdCRIPTO). Error bars indicate ±SD (n=3).

CRIPTO and GRP78 expression in human HCC

Based on the induction of CSC and EMT markers *in vivo* and *in vitro*, the expression levels of CRIPTO and GRP78 in human HCC liver specimens were evaluated. Aetiopathological heterogeneity in HCC was taken into account during the selection of HCC patient material; in this study we assessed specimens from HCV infection-driven HCC (HCV-HCC) or alcoholic liver disease-driven HCC (ALD-HCC). Adjacent tissue to the resected tumor, derived from the same patient, was used for comparison (control). We found that CRIPTO protein levels are lower in the adjacent non-tumor tissue compared to the tumor area in 50% of the patients with HCV-related and in all ALD-related HCC patients (n=4 per group) (**Fig.3A-B, 3D-E**). In tumor tissue areas, higher CRIPTO expression levels were observed at the vicinity of the stroma (**Fig.3A, 3D**). For comparison, samples from patients with only HCV infection and without detected signs of cirrhosis or HCC were also analysed and revealed low to none CRIPTO and GRP78 expression (**Fig.3B-C**). GRP78 is upregulated in HCC tissue areas in 25%

of the analysed HCV-related HCC patient samples (**Fig.3A,C**) and in 50% of the analysed ALD-related HCC tissues compared to adjacent non-tumorous tissue (**Fig.3D,F**).
To assess functional effects exerted by CRIPTO in HCC, we generated a stable HepG2- CRIPTO cell line by lentiviral transduction (LV-MOCK, LV-CRIPTO). The overexpression of CRIPTO was confirmed at the mRNA level by quantitative PCR (**Fig.4A**). Associated NODAL pathway members (NODAL, ALK4, LEFTY) and GRP78 were also upregulated in the LV-CRIPTO HepG2 (**Fig.4B-E**). Moreover, proliferation (MTS assay), migration (transwell assay) and wound closure assay showed that the HepG2-CRIPTO cells become more proliferative (**Fig.4F**) and motile (**Fig.4G-H**). Consistent with the acquisition of invasive and mesenchymal properties CRIPTO overexpressing cells show downregulation of E-CADHERIN (**Fig.5A**), upregulation of EMT markers (VIMENTIN, ZEB-1, ZEB-2, TWIST and SNAIL-2) (**Fig.5B-F**) and increased CSC marker (EpCAM, BMI-1 and CD44) expression (**Fig.5G-I**).

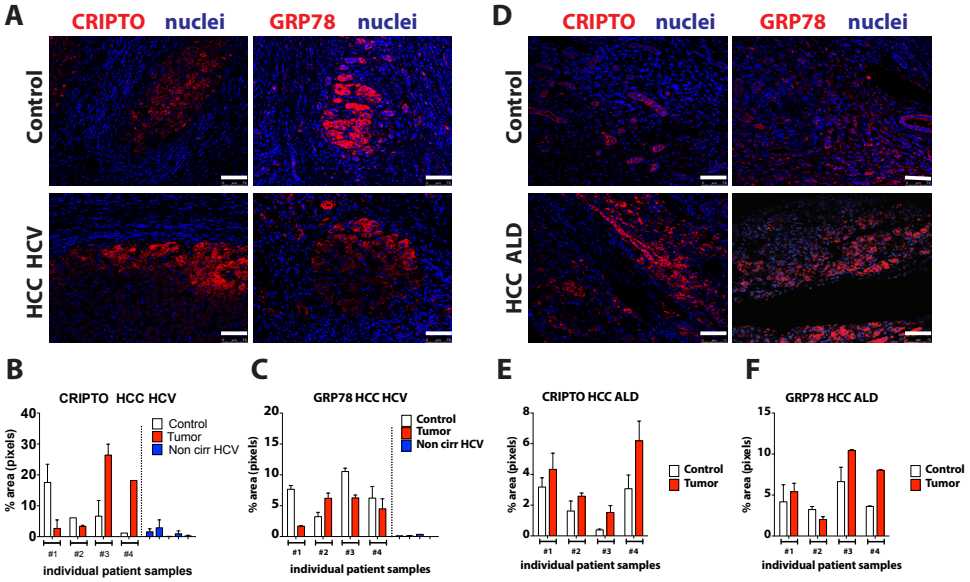

Fig.3. Expression of CRIPTO and its interaction partner GRP78 in human HCC liver tissues
(A). Representative immunofluorescence images of CRIPTO and its interaction partner GRP78 staining in human liver sections from HCV-derived HCC tissue (HCV infection-driven) and adjacent non-tumor control tissue from the same patient. Nuclei are stained with TO-PRO-3 (blue). Scale bars 75 μm. (B). Quantification of CRIPTO and (C). GRP78 protein expression as assessed by immunofluorescence in tumor HCC HCV (Tumor) and in adjacent non-tumor tissue (Control) from the same patient (n=4). Liver tissue from patients with HCV infection but absence of cirrhosis (non-cirrhotic HCV, n=4) was used for comparison. The percentage of positive pixel area was an average from two-four focal areas per section. Each bar represents values from each patient. Error bars indicate ±SD. (D). Representative immunofluorescence images of CRIPTO and its interaction partner GRP78 protein expression in human liver sections from alcoholic liver disease (ALD)-derived HCC tissue and adjacent non- tumor control tissue from the same patient. Nuclei are stained with TO-PRO-3 (blue). Scale bars 75 μm. (E). Quantification of CRIPTO and (F) GRP78 protein expression as assessed by immunofluorescence in tumor HCC ALD (Tumor), adjacent non-tumor tissue (Control) from the same patient (n=4). The percentage of positive area (pixels) was the average from two-four focal areas per section. Each bar represents values from each patient. Error bars indicate ±SD.

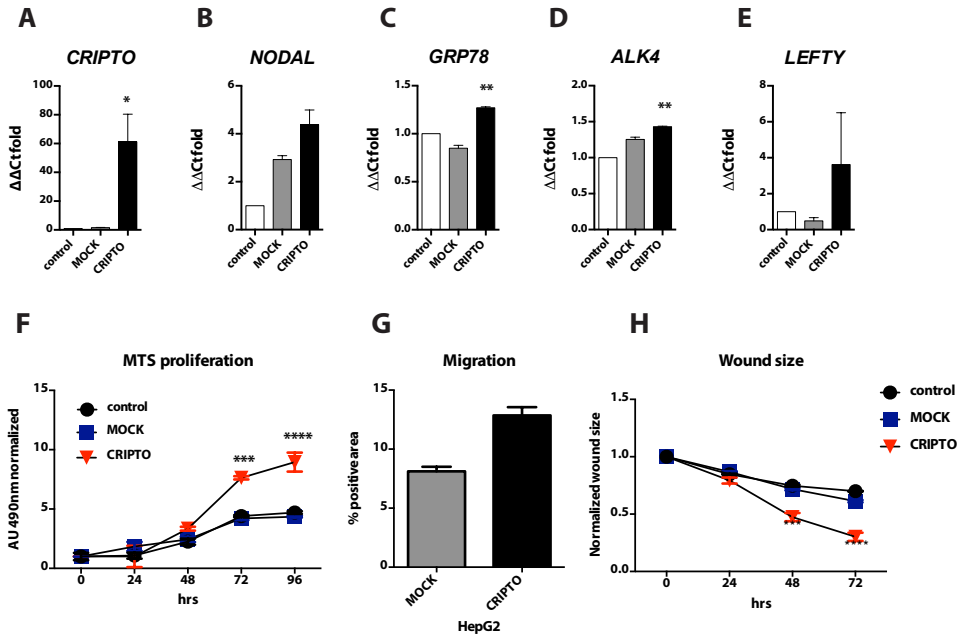

Fig.4. *In vitro* effects of stable overexpression of CRIPTO in HepG2 cells

(A-E). Quantitative PCR for mRNA expression of Cripto associated members of the NODAL and GRP78 pathways in wild type HepG2 cells; control, stably overexpressing Mock construct after lentivirus transduction (MOCK) and stably overexpressing CRIPTO (CRIPTO). (A). CRIPTO, (B). NODAL, (C). GRP78, (D). ALK4 and (E). LEFTY mRNA expression (n=3, ±SEM). Values are normalized to *β-actin* and to control sample (ΔΔCT fold expression). (F). Metabolic activity MTS assay (24, 48, 72, 96 hours) was performed in control, MOCK and CRIPTO overexpressing HepG2 cells. Accumulation of MTS was measured based on absorbance at 490 nm. Values are normalized to the basal measurements at 0 hours after cell seeding. Graph represents values for three independent experiments (n=3). Error bars indicate SEM. p value < 0.001 (***), < 0.0001 (****). (G). Transwell migration assay of LV-MOCK and LV-CRIPTO overexpressing HepG2 cells; quantification of percentage (%) of positive area of migrated cells (Crystal violet cell dye) was performed in two independent experiments. Error bars indicate ±SEM. (H). Cell motility was assessed in wound healing (scratch) assay. Wound size was quantified in a time-dependent manner (0, 24, 48 and 72 hours) in two independent experiments. Error bars indicate ±SEM.

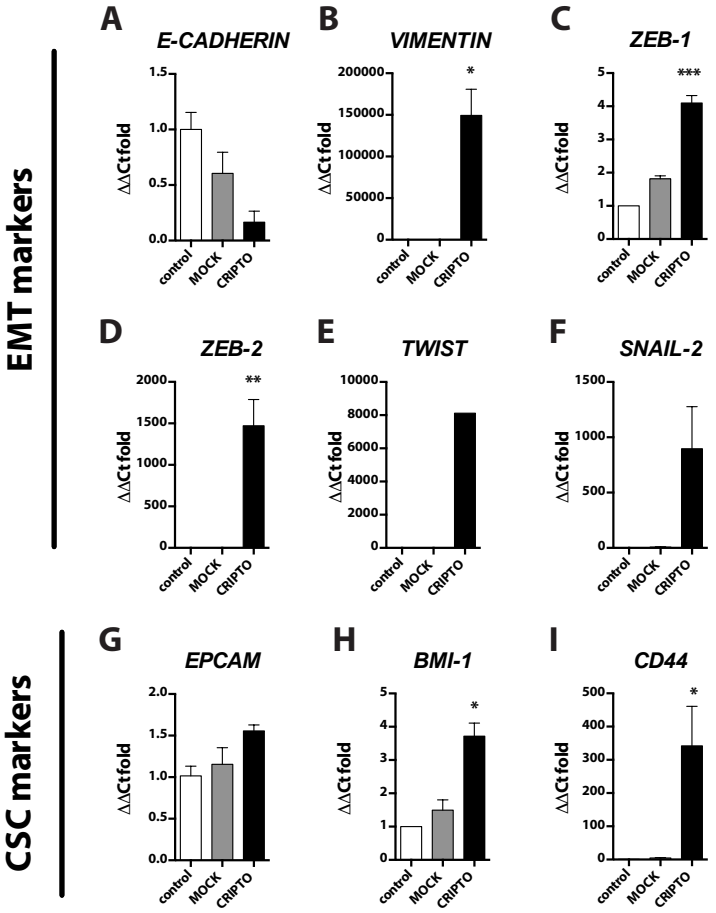

Fig.5. Expression of EMT and CSC markers in HepG2 cells upon stable overexpression of CRIPTO

(A-F). The levels of mRNA expression of epithelial-to-mesenchymal (EMT) markers in control, MOCK and CRIPTO-overexpressing HepG2 cells was assessed by quantitative PCR; (A). E-CADHERIN, (B). VIMENTIN, (C). ZEB-1, (D). ZEB-2, (E). TWIST, (F). SNAIL2. (G-I). mRNA expression levels of cancer stem cell (CSC) markers; (G). EPCAM, (H). BMI-1, (I). CD44. All values are normalized to *β-actin* and to control sample (ΔΔCT fold expression), n=3, ±SEM.

Discussion

The ability of quiescent hepatocytes to become proliferative and replace the damaged cells, both of the hepatocyte and cholangiocyte lineage, is at the foundation of liver regeneration[41]. In addition, hepatic stellate cells and Kupffer cells orchestrate wound healing response by the secretion of cytokines, removal of dead cells and extracellular matrix restoration. The general perception is that liver progenitor cells (oval cells) reside in the bile duct (at the portal triad) and their role is largely compensated by hepatocytes, bone marrow- derived fibrocytes and possibly hematopoietic stem cells. Oval cells typically are only detectable upon chronic liver injury or carcinogenesis and not upon acute CCl_4 damage[43]. However, in our model we observed reactivation of CK19 and AFP, markers of oval cells, followed by bile duct proliferation, a process associated with oval cell activation usually observed after partial hepatectomy or bile duct ligation[42,44,45]. Oval cell marker AFP has important functions during embryogenesis, it is postnatally silenced and re-expression often drives clonal expansion of oval cell-derived tumors[43,46]. AFP has been discarded from diagnostic schemes in recent guidelines due to the limited sensitivity[4,47].

Here we report preliminary evidence that (1) pluripotency-associated protein CRIPTO is reactivated *in vivo* at early stages after acute liver injury, (2) CRIPTO overexpression induces bile duct reaction and AFP upregulation, (3) acute liver injury may also elicit the activation of oval cells. The rapid dynamics of CRIPTO and AFP expression and downregulation *in vivo* suggest that their expression levels are tightly regulated in order to induce a short-term cellular response; in this case perhaps a beneficial role in regenerative response. We speculate that due to the oncogenic role of high AFP levels in the liver and of CRIPTO in other tissues, both proteins are silenced in the adult organism to prevent abnormal activation of oval cells and tumor formation.

In the majority of human HCV- related HCC and ALD-related HCC tissue samples, the levels of CRIPTO were elevated in the tumor area compared to adjacent non-tumorous tissue from the same patient. CRIPTO- GRP78- mediated AKT signaling has been found to contribute to tumorigenesis[24], thus, we assessed the expression levels of GRP78 in human HCC specimens. Indeed, higher levels of GRP78 were detected in 50% of the tumor tissues of the ALD-HCC group and in 25% of the HCV-HCC group, similar to CRIPTO. However, 75% of HCV-related HCC showed reduced GRP78 expression that coincides with previous findings showing that GRP78 has a protective role in the liver, against steatosis and cancer.

The location of CRIPTO in the hepatocytes, in particular those at the border between tumor nodule and stroma, has led us to the hypothesis that CRIPTO may promote invasiveness. Stable overexpression of CRIPTO in HepG2 cells induces their proliferative and migratory potential and is associated with an increase of EMT transcription factor and mesenchymal marker expression. Transient and stable overexpression of CRIPTO upregulates NODAL, LEFTY and GRP78, thus more aggressive, EMT-like phenotype of these cells may be attributed to either or both GRP78 and canonical NODAL signaling, however, further investigations are required.

In summary, this study provides supportive evidence for a novel role of developmental protein Cripto during progenitor cell activation during acute liver injury, suggesting that common developmental programs also regulate liver development and adult liver injury response. CRIPTO expression correlates with progression to human hepatic carcinogenesis in response to HCV hepatitis infection and alcoholic disease. The implication of fetal oncoprotein Cripto in the early response to acute liver injury and in advanced liver cancer may indicate

that CRIPTO is part of the missing link between acute and chronic liver injury, progression to cirrhosis and further to cancer formation.

Acknowledgements

We thank Midory Thorikay for technical assistance with the adenovirus construct, Boudewijn Kruithof, Peter Gray and Eugenio Zoni for critical discussions.

References

1. Attwa, M.H. and S.A. El-Etreby, Guide for diagnosis and treatment of hepatocellular carcinoma. World J Hepatol, 2015. 7(12): p. 1632-51.
2. El–Serag, H.B. and K.L. Rudolph, Hepatocellular carcinoma: epidemiology and molecular carcinogenesis. Gastroenterology, 2007. 132(7): p. 2557-2576.
3. Llovet, J.M., et al., Sorafenib in advanced hepatocellular carcinoma. N Engl J Med, 2008. 359(4): p. 378-390.
4. European Association for the Study of the, L., R. European Organisation for, and C. Treatment of, EASL–EORTC Clinical practice guidelines: management of hepatocellular carcinoma. J Hepatol. . 56(4): p. 908-943.
5. Rahimi, R.S. and J.F. Trotter, Liver transplantation for hepatocellular carcinoma: outcomes and treatment options for recurrence. Ann Gastroenterol., 2015. 28(3): p. 323-330.
6. Behne, T. and M.S. Copur, Biomarkers for hepatocellular carcinoma. Int J Hepatol., 2012. 2012: p. 7.
7. Petersen, B.E., V.F. Zajac, and G.K. Michalopoulos, Hepatic oval cell activation in response to injury following chemically induced periportal or pericentral damage in rats. Hepatology, 1998. 27(4): p. 1030-1038.
8. Dooley, S. and P. ten Dijke, TGF-β in progression of liver disease. Cell Tissue Res, 2012. 347(1): p. 245-56.
9. Battaglia, S., et al., Liver cancer-derived hepatitis C virus core proteins shift TGFβ responses from tumor suppression to epithelial-mesenchymal transition. PLoS One, 2009. 4(2): p. e4355.
10. Song, B.-C., et al., Transforming growth factor-β1 as a useful serologic marker of small hepatocellular carcinoma. Cancer, 2002. 94(1): p. 175-180.
11. Park, Y.N., et al., Expression of Smad7 in hepatocellular carcinoma and dysplastic nodules: resistance mechanism to transforming growth factor-β. Hepatogastroenterology, 2004. 51(56): p. 396-400.
12. Serova, M., et al., Effects of TGF-β signaling inhibition with galunisertib (LY2157299) in hepatocellular carcinoma models and in ex vivo whole tumor tissue samples from patients. Oncotarget2015(Epub).
13. Paik, S.Y., et al., Expression of transforming growth factor-β1 and transforming growth factor-β receptors in hepatocellular carcinoma and dysplastic nodules. Mod Pathol, 2003. 16(1): p. 86-96.
14. Torbenson, M., et al., Smad4 overexpression in hepatocellular carcinoma is strongly associated with transforming growth factor β II receptor immunolabeling. Hum Pathol., 2002. 33(9): p. 871-876.
15. Sun, C., et al., NANOG promotes liver cancer cell invasion by inducing epithelial–mesenchymal transition through NODAL/SMAD3 signaling pathway. Int J Biochem Cell Biol., 2013. 45(6): p. 1099-1108.
16. Lonardo, E., et al., Nodal/Activin signaling drives self-renewal and tumorigenicity of pancreatic cancer stem cells and provides a target for combined drug therapy. Cell Stem Cell, 2011. 9(5): p. 433-46.
17. Wakefield, L.M. and C.S. Hill, Beyond TGFβ: roles of other TGFβ superfamily members in cancer. Nat Rev Cancer, 2013. 13(5): p. 328-341.
18. Gray, P.C., et al., Cripto binds Transforming growth factor β (TGF-β) and inhibits TGF-β signaling. Mol Cell Biol., 2006. 26(24): p. 9268-9278.

19. Gray, P.C., C.A. Harrison, and W. Vale, Cripto forms a complex with activin and type II activin receptors and can block activin signaling. Proc Natl Acad Sci U S A., 2003. 100(9): p. 5193-5198.
20. Gray, P.C. and W. Vale, Cripto/GRP78 modulation of the TGF-β pathway in development and oncogenesis. FEBS Lett, 2012. 586(14): p. 1836-1845.
21. Klauzinska, M., et al., The multifaceted role of the embryonic gene Cripto-1 in cancer, stem cells and epithelial-mesenchymal transition. Semin Cancer Biol., 2014. 29(0): p. 51-58.
22. Bianco, C., et al., A Nodal- and ALK4-independent signaling pathway activated by Cripto-1 through Glypican-1 and c-Src. Cancer Res, 2003. 63(6): p. 1192-1197.
23. Kruithof-de Julio, M., et al., Regulation of extra-embryonic endoderm stem cell differentiation by Nodal and Cripto signaling. Development, 2011. 138(18): p. 3885-3895.
24. Spike, Benjamin T., et al., CRIPTO/GRP78 signaling maintains fetal and adult mammary stem cells ex vivo. Stem Cell Reports., 2014. 2(4): p. 427-439.
25. Xu, C.-H., et al., Elevated expression of Cripto-1 correlates with poor prognosis in non-small cell lung cancer. Tumour Biol., 2014. 35(9): p. 8673-8678.
26. Cocciadiferro, L., et al., Profiling cancer stem cells in androgen-responsive and refractory human prostate tumor cell lines. Ann N Y Acad Sci. , 2009. 1155(1): p. 257-262.
27. Terry, S., et al., CRIPTO overexpression promotes mesenchymal differentiation in prostate carcinoma cells through parallel regulation of AKT and FGFR activities. Oncotarget, 2015. 6(14): p. 11994-2008.
28. D'Antonio, A., et al., Transforming growth factor alpha, amphiregulin and cripto-1 are frequently expressed in advanced human ovarian carcinomas. Int J Oncol, 2002. 21(5): p. 941-8.
29. Fujii, K., et al., Expression of CRIPTO in human gall bladder lesions J Pathol., 1996. 180(2): p. 166-168.
30. Giorgio, E., et al., Cripto haploinsufficiency affects in vivo colon tumor development. Int J Oncol., 2014. 45(1): p. 31-40.
31. Strizzi, L., et al., The significance of a Cripto-1-positive subpopulation of human melanoma cells exhibiting stem cell-like characteristics. Cell Cycle, 2013. 12(9): p. 1450-1456.
32. Tysnes, B.B., et al., Age-dependent association between protein expression of the embryonic stem cell marker Cripto-1 and survival of glioblastoma patients. Transl Oncol., 2013. 6(6): p. 732-741.
33. Steelman, L.S., et al., Roles of the Raf/MEK/ERK and PI3K/PTEN/Akt/mTOR pathways in controlling growth and sensitivity to therapy-implications for cancer and aging. Aging (Albany NY), 2011. 3(3): p. 192-222.
34. Ji, C., et al., Liver-specific loss of GRP78 perturbs the global unfolded protein response and exacerbates a spectrum of acute and chronic liver diseases. Hepatology 2011. 54(1): p. 229-239.
35. Kuo, T.-C., et al., A unique P-glycoprotein interacting agent displays anticancer activity against hepatocellular carcinoma through inhibition of GRP78 and mTOR pathways. Biochem Pharmacol., 2011. 81(9): p. 1136-1144.
36. Chen, W.-T., et al., GRP78 as a regulator of liver steatosis and cancer progression mediated by loss of the tumor suppressor PTEN. Oncogene, 2014. 33(42): p. 4997-5005.
37. Shayakhmetov, D.M., et al., Analysis of adenovirus sequestration in the liver, transduction of hepatic cells, and innate toxicity after injection of fiber-modified vectors. J Virol. , 2004. 78(10): p. 5368-5381.
38. Karkampouna, S., et al., Inhibition of TGFβ type I receptor activity facilitates liver regeneration upon acute CCl4 intoxication in mice. Arch Toxicol., 2015: p. 1-11.
39. Zoni, E., et al., miR-25 modulates invasiveness and dissemination of human prostate cancer cells via regulation of alphav- and alpha6-integrin expression. Cancer Res, 2015. 75(11): p. 2326-36.
40. Bianco, C., et al., Role of Cripto-1 in stem cell maintenance and malignant progression. Am J Pathol., 2010. 177(2): p. 532-540.
41. Fausto, N. and J.S. Campbell, The role of hepatocytes and oval cells in liver regeneration and repopulation. Mech Dev. , 2003. 120(1): p. 117-130.

42. Limaye, P.B., et al., Expression of hepatocytic- and biliary-specific transcription factors in regenerating bile ducts during hepatocyte-to-biliary epithelial cell transdifferentiation. Comp Hepatol., 2010. 9: p. 9-9.
43. Dabeva, M.D., et al., Models for hepatic progenitor cell activation. Proc Soc Exp Biol Med, 1993. 204(3): p. 242-52.
44. Liu, Z., et al., Interleukin-6, hepatocyte growth factor, and their receptors in biliary epithelial cells during a type i ductular reaction in mice: Interactions between the periductal inflammatory and stromal cells and the biliary epithelium. Hepatology, 1998. 28(5): p. 1260-1268.
45. Yoshioka, K., et al., Cell proliferation activity of proliferating bile duct after bile duct ligation in rats. Vet Pathol., 2005. 42(3): p. 382-385.
46. Kuhlmann, W.D. and P. Peschke, Hepatic progenitor cells, stem cells, and AFP expression in models of liver injury. Int J Exp Pathol, 2006. 87(5): p. 343-59.
47. Bruix, J. and M. Sherman, Management of hepatocellular carcinoma. Hepatology, 2005. 42(5): p. 1208-1236.